Modelling historical global tsunamis with TELEMAC

Thomas Saillour[1], Giovanni Cozzuto[1] , Giorgio Lupoi[1], Giovanni Cuomo[1], Sebastien E. Bourban[2]
tsaillour@studiosperi.it, gcozzuto@studiosperi.it, gcuomo@studiosperi.it, Palermo, Italy
sebastien.bourban@edf.fr, Paris, France
[1]: Studio Speri Società di Ingegneria S.r.l., Rome, Italy
[2]: EDF R&D LNHE / LHSV, Paris, France

Abstract – **This paper presents the results of a highly resolved metocean model of the world oceans and its application to the modelling of a selection among the most energetic transoceanic tsunamis, with particular emphasis on the Tōhoku tsunami. Thanks to its adaptive resolution and new features implemented in the source code, the model is able to better represent the complexity of the seismic source and predict the tsunami wave characteristics around the globe. After a short introduction and discussion of the possible representation of the tsunami source terms, the paper illustrates initial results and the accuracy of the model and introduces possible ways of improving the model performances, which includes modelling simultaneously the evolution of different physical processes (tides, surges, tsunamis) thanks to the versatility of the TELEMAC solver suite [2][1].**

Keywords: global, tsunamis, validation, TELEMAC-2D

I. INTRODUCTION

Predicting natural disasters and their likely impact on the natural and built environment is a fundamental step towards the development of better informed global risk management strategies, contributing to worldwide risk reduction and mitigation. In this context, accurate and effective modelling of tsunamis is not only vital for the safety of coastal communities, but contributes to the creation of safer and more resilient world.

The capacity of the TELEMAC solver to qualitatively model tsunamis at a global scale has already been proven in previous publications [4][7]. The purpose of this paper is to illustrate the implementation of state-of-art generation techniques and quantitatively compare the modelled tsunami waves heights with the DART buoys system.

Traditionally, seismically generated tsunamis modelling is initiated using the Okada model to translate earthquakes parameters (that can be inferred using, for example, joint earthquake source inversion techniques [3]), onto initial instantaneous deformation of sea bottom and/or ocean surface. Having the most accurate source possible contributes to improving the ability of any model to accurately represent the dynamics of the tsunami. With this in mind, we add new features in the source code of TELEMAC-2D, features that will be described further down the article. All the modelling described in this paper has been done using TELEMAC-2D.

The goal of this of the paper is trifold: (1) prove that TELEMAC can accurately predict Tsunami wave propagations, (2) demonstrate that tsunamis can be run at a global scale along with other processes – for instance tides – and (3) identify the weaknesses of the solver in order to propose the next axis of development for tsunami applications. The ultimate achievement being: bringing the solver to a sufficient level of accuracy to reliably provide tsunami alerts or risk assessments for national entities and communities.

II. TSUNAMIS

A succinct literature review has been undertaken in order to identify the most relevant tsunamis for this study. In total, more than 2700 events are registered on the NGDC/WDS Global Historical Tsunami Database [5].

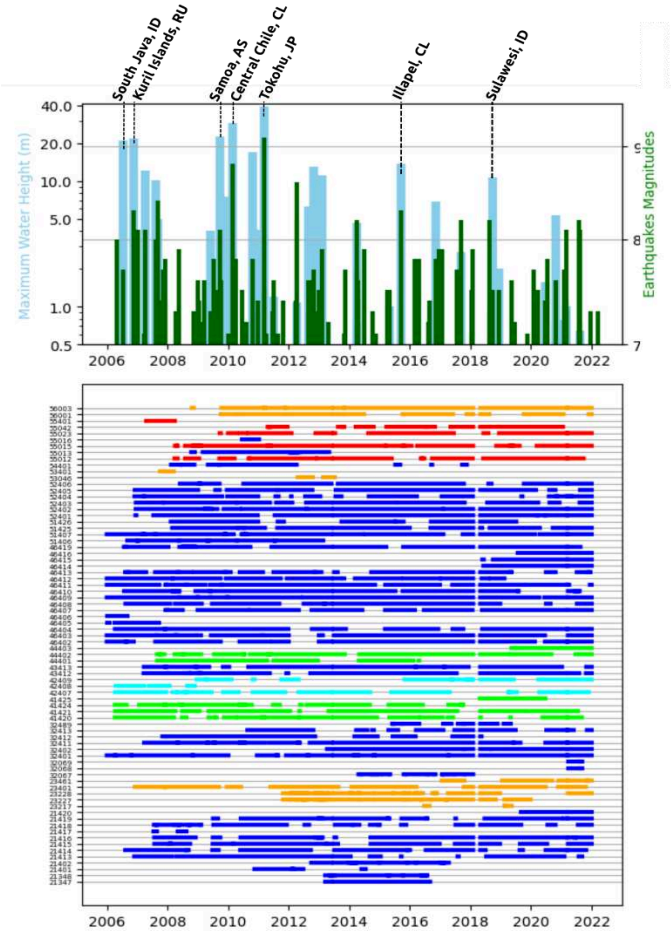

Figure 1. Top: tsunami runups in blue and earthquakes magnitudes in green. Bottom: superposition of the events with the DART system activity. Blue, green, orange, cyan and red colors indicate DART buoys in Pacific, Atlantic, Indian, Carribbean and Tasman sectors.

Figure 1 compiles all the highest observed runups and matched their timeline with the DART buoys activity in every ocean. The following criteria have been defined in order to refine the selection over the whole database: (1) the event has happened after the launch of the DART program in 2006, (2) the event had a runup higher than 10m and (3) the earthquake that generated the tsunami had a magnitude higher than 7.0 on the Richter scale. For every event matching the previously defined criteria (a dozen), the signal in the hours following the tsunami has been undertaken for each active buoy.

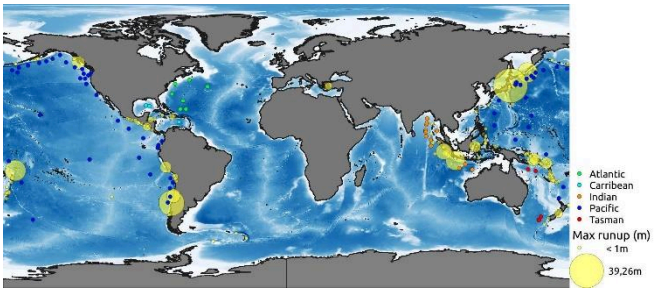

Figure 2. Tsunami runups since 2006 in yellow. Blue, green, orange, cyan and red circles indicate DART buoys in Pacific, Atlantic, Indian, Carribbean and Tasman sectors as referenced in Figure 1.

Figure 1 shows the repartition of the DART buoys around the world and the distribution of tsunami events since 2006, represented by their associated maximum runup. Among all events, only four of them had data recorded by more than ten DART buoys. Global tidal records can also be found [6], but the scope of this paper is to compare the deep water wave heights before investigating runup levels at tidal stations.

As the selection shrunk to the four events detailed in Table I, four global models have been setup. However, to illustrate the capacity of TELEMAC to quantitatively predict tsunamis (and also for the sake of the length of this paper), the results of only one study case will be fully detailed; the event with the biggest number of observations i.e. the Tōhoku tsunami in February 2011. The three other case studies will have their preparation and meshing detailed as a demonstration of the ability to model tsunamis at a global scale.

Table I Tsunami events and number of active DART buoys

Event	Time (UTC)	Magnitude	Number of buoys records
Tōhoku Japan	2011-03-11 05:46:24	9.1	28
Central Chile	2010-02-27 06:34:23	8.8	23
Illapel, Chile	2015-09-16 22:54:32	8.3	24
Samoa	2009-09-29 17:48:10	8.1	16

III. MESHING THE WORLD OCEANS

Since the scope of the model is to be able to account for the tsunami wave heights at a global scale, only global databases have been used for the setup of the model. The General Bathymetric Chart of the Oceans, developed by the International Hydrographic Organization (IHO) and the Intergovernmental Oceanographic Commission (IOC), provides gridded bathymetry data which covers lands and oceans around the whole globe with a resolution of ~ 0.004° (~ 450m). As mentioned in [4], unstructured grid generated for the study needs to resolve multiphysics metocean processes at different scales. Thus, the triangle mesh has an adaptive resolution, and an optimised procedure has been developed to size the mesh elements to effectively resolve the features of the bathymetry and the coastlines.

A tailored mesh has been created for each event, by enhancing its resolution in the vicinity of the source, in order to better model the initial conditions according to the sub-fault models, but also to better model the wave heights at the first location of impact of the tsunami. For all meshes, a common global mesh with a target resolution of 10km at the coastlines has been associated with a higher grade mesh with a resolution from 2km up to 450m close to the shores where the tsunami hit the coastlines first. The highest resolution is in fact limited by the input data (i.e. the resolution of the GEBCO bathymetry i.e. 450m).

Using a better defined bathymetry would have permitted a higher and better resolution of the final mesh, however evaluating the tsunami surge and inundations on the coastlines is not the scope of this paper… yet (see chapter VII: Perspectives). The number of nodes and elements of each unstructured mesh is specified in Table II.

Table II Tsunami events and number of active DART buoys

Event	Number of elements	Number of triangles
Tōhoku Japan	1 359 682	695 042
Central Chile	1 328 456	680 911
Illapel, Chile		
Samoa	1 054 588	543 345

Although there were four events selected, two of them happened in Chile. This is the reason why only *three* different meshes have been generated. For the Chilean configuration, the refinement in the resolution has been done so that both of the events (from 2010 or 2015) could be modelled using the same and only grid, represented in the centre inset of Figure 3.

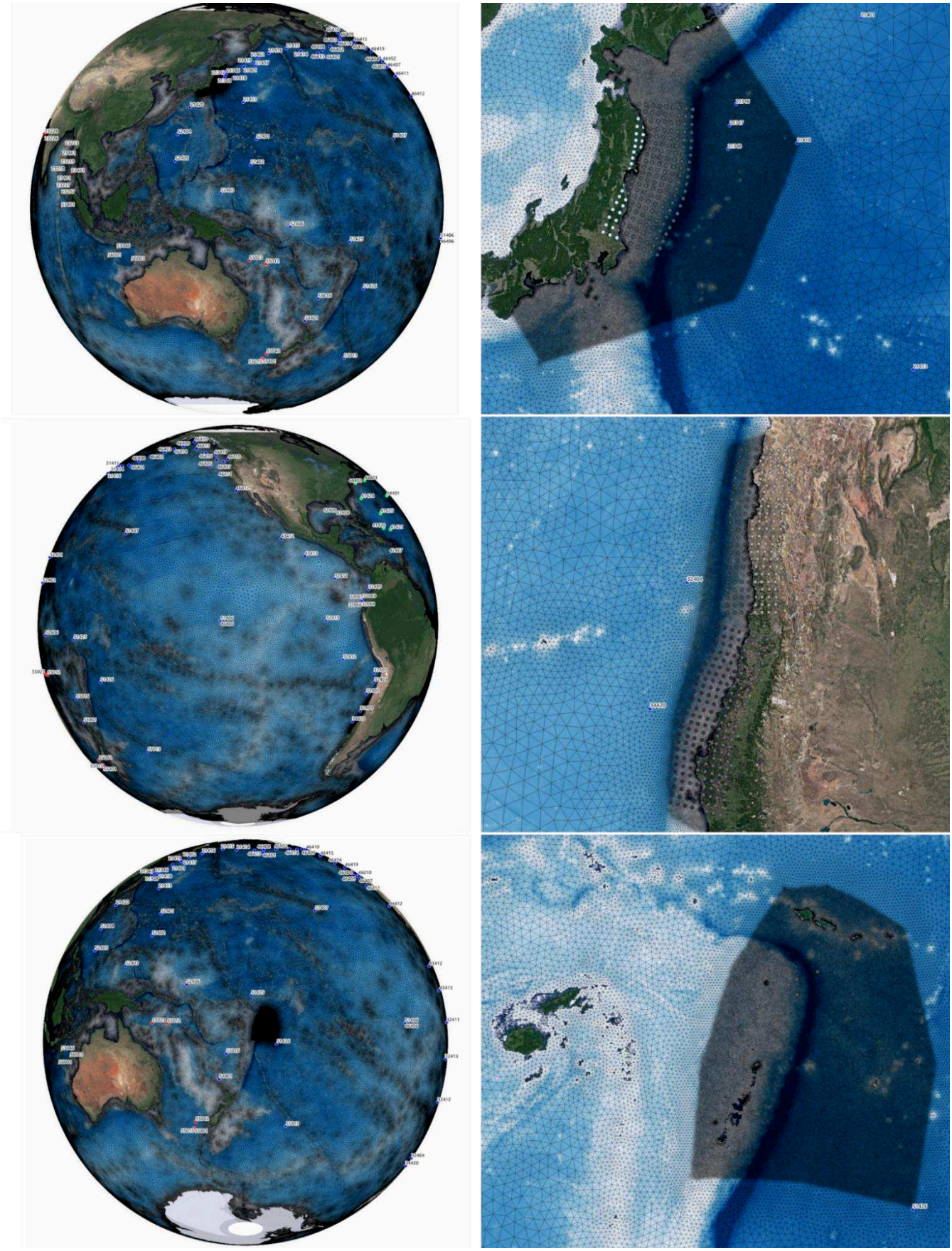

Figure 3. Unstructured grids for four events: Tōhoku 2011 (top insets), Chile 2010 and 2015 (centre) and Samoa 2009 (bottom insets). The fault models have been indicated with the points laying under the mesh

IV. MODELLING TSUNAMIS IN TELEMAC-2D

A. *The Okada model*

The Okada model [8] is widely used in earth and ocean science for specifying the deformations induced by seismic events. The Okada generator has been implemented since version v7p2 of the TELEMAC system in 2012 [7]. The seabed deformation is characterized by its focal depth D, its fault length L and width W, its dislocation (or slip) u, its strike direction d, its dip angle δ, its slip angle (or rake) ϕ, its epicentre coordinates (lat_E, lon_E) and the size E of the ellipse of influence of the tsunami. Tsunamis are enabled in TELEMAC-2D (and TELEMAC-3D) by the following keywords:

- ✓ OPTION FOR TSUNAMI GENERATION**; and**
- ✓ PHYSICAL CHARACTERISTICS OF THE TSUNAMI

A single fault model will then induce the following vertical bottom displacement ζ along x and y:

$$\zeta(x,y) = O(x,y,D,W,L,\delta,d,\phi,u,lat_E,lon_E,E) \quad (1)$$

with O being the Okada solution, (x,y) the latitude and longitude of a point in the model, and the ten input parameters for the Okada model, in the order they were defined above.

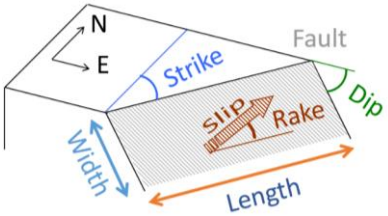

Figure 4. Tsunami characterisation and parameters used in Okada's solution

The Okada model generator implemented in TELEMAC only allows the generation of single faults source events and imposes the deformation ζ as an initial state condition at the beginning of the model. To obtain results comparable with the other software used in the literature [9][10][11], it was needed to add multi-source events but also enabling the *active* deformation of seafloor.

B. *Multi-faults tsunami sources*

Implementing multiple sources is rather simple, as is consists in defining the local deformation of the bottom displacement from each contribution of the finite fault model[12]. If the fault plane is discretised in N_x sub-faults along strike and N_y sub-faults along the dip angle, we define the final deformation of the earth surface as follows:

$$\zeta(x,y) = \sum_{i=1}^{Nx \times Ny} O(x,y,D_i,W_i,L_i,\delta_i,d_i,\phi_i,u_i,lat_i,lon_i,E_i) \quad (2)$$

If there are overlaps between the sub-faults, all the contributions from the co-seismic parameters of each fault are summed together. The following figure shows the difference between a single fault model and three different multi-faults models for the Tōhoku 2011 tsunami.

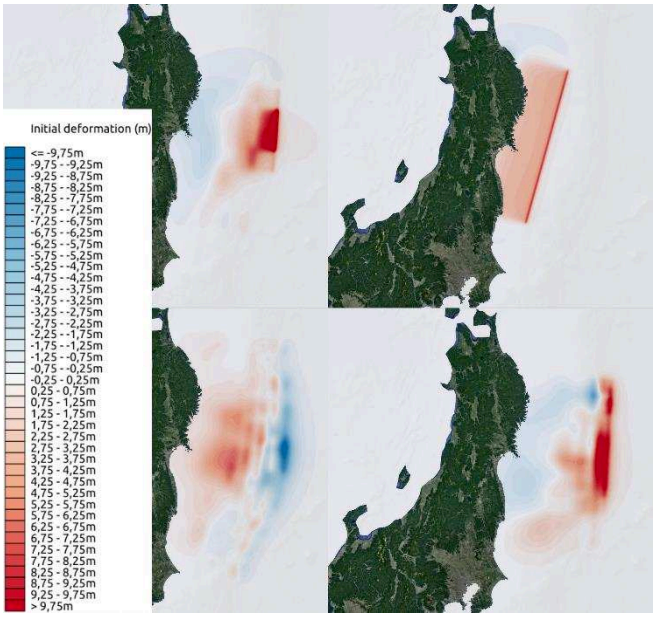

Figure 5. Representations of the initial condition for three different multifaults and one single fault models for the Tōhoku tsunami in 2011; Fuji 2011[13] with 40 sub-faults (top left), Ravi 2013[14] with one single fault (top right), Romano 2012[15] with 189 sub-faults (bottom left) and Yamasaki 2018[16] with 240 faults (bottom right).

A comparison between the signals generated by the different tsunami sources has been done for the closest active buoy to the tsunami source (DART 21418) and is represented in the next Figure 6. The single fault source from Ravi 2013 [14] will then be ignored for the Tōhoku case study as not fit enough to describe properly the bottom deformation for the initial state of the simulation.

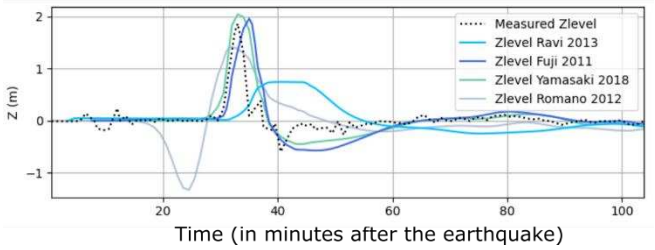

Figure 6. Signals measured and modeled at the closest active buoy to the earthquake epicenter (DART 21418).

C. *Passive and active tsunami generation*

The Okada generator routine uses Okada's solution as initial condition for the free surface, while all velocities are set to zero. We will follow the example of Mitsotakis[17], who defines this as the *passive* generation of a tsunami. The equations of the free surface at t = 0 are as follows:

$$\eta(x, y, 0) = \zeta(x , y) \; ; \; \mathbf{u}(x, y, 0) = 0 \quad (3)$$

with ζ(x , y) defined in equation (2)

The *active* generation is achieved by specifying zero initial conditions for both the free surface and the velocities and assuming that the bottom is changing over time. We define the sub-faults activation times t_i in order to trigger the

sub-faults ruptures in a desynchronized way. The bottom motion depends on the rising time t_r of the fault rupture. The deformation of the seabed is expressed as follows:

$$h(x,y,t) = D(x,y) + \sum_{i=1}^{N_x \times N_y} \mathcal{H} \cdot T \cdot O_i(x,y,\dots) \qquad (4)$$

where $\mathcal{H} = \mathcal{H}(t - t_i, t_r)$ is the Heaviside step function, and $T = T(t - t_i, t_r)$ is the trigonometric scenario of the bottom motion (Dutykh 2013[12]).

Although the literature cited above [12][17] refers to applications based on the use of numerical models solving the Boussinesq equations, the active generation – that is applying a dynamically changing seabed condition – is also valid for modelling using TELEMAC, as it adds velocities to the seabed deformation and thus generates bigger tsunami waves. The total time of the sea floor deformation (or rising time t_r) will impact the speed of the bathymetric motion and hence the amplitude of the tsunami wave.

The Figure 7 shows the influence of the rising time value on the amplitude of the modelled free surface. We also tried an instantaneous deformation of the seabed as it is used in some of the publications cited in this paper [13].

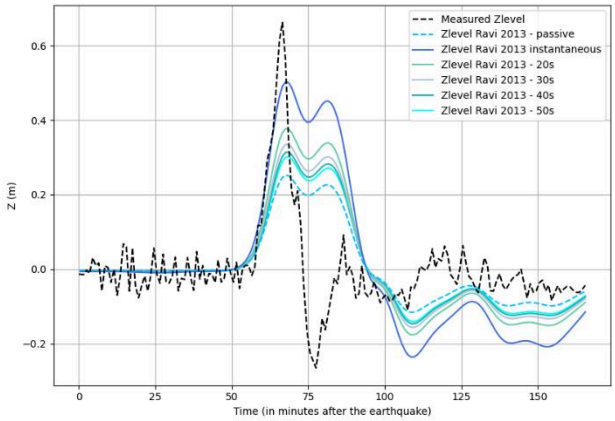

Figure 7. Influence of the rising time on the amplitude of the tsunami. Comparison done for the single fault description of the Tōhoku earthquake at one of the nearest active buoys (DART 21401).

We have introduced two new parameters (t_i and t_r) that we use for the generation of tsunamis. Each subfault is now characterized by 12 parameters: t_i, t_r, D_i, W_i, L_i, δ_i, d_i, ϕ_i, u_i, lat_i, lon_i and E_i which are the discretized parameters defined in (1) preceded by the activation time t_i and the rising time t_r of each subfault.

V. VALIDATION OF THE RESULTS

A. *Tōhoku 2011*

For the 2011 Tōhoku earthquake of 2011, three different multi-faults models have been considered and are detailed in the Table III. All the detailed information about the faults models is open source and available under the section "Supplementary Information" for all publications. (Or directly in a table of the publication for Fuji 2011). An *active* generation has been implemented for all three faults models. In the cited publications, Yamasaki 2018 [16] uses 32 seconds rising times t_r for the high resolution fault model (with 240 subfaults) with different initial activation times t_i, with a whole faulting time of 150 seconds, Fuji 2011[13] assumes a instantaneous deformation and Romano 2012[15] does not mention it. Following an iterative procedure of calibration, we finally also assumed an instantaneous deformation for all models.

Table III Source fault models used for tsunami generation in TELEMAC

Fault model	Number of faults	Size of the subfaults
Romano 2012 [15]	189	25km x 25km
Yamasaki 2018[a] [16]	240	20km x 20km
Fuji 2011 [13]	40	50km x 50km

a. Here we use the "Initial model P-MOD2. i.e. the 240 subfaults high resolution model. The authors also provide a downsampled and calibrated version of the model (TMOD model: 60 subfaults of 40km×40km). Both models gave us really similar results.

The source fault model propagation in Figure 8 corresponds to the Yamasaki 2018 configuration. Only the active DART buoys that recorded a tsunami signal are displayed on the map with their identification number.

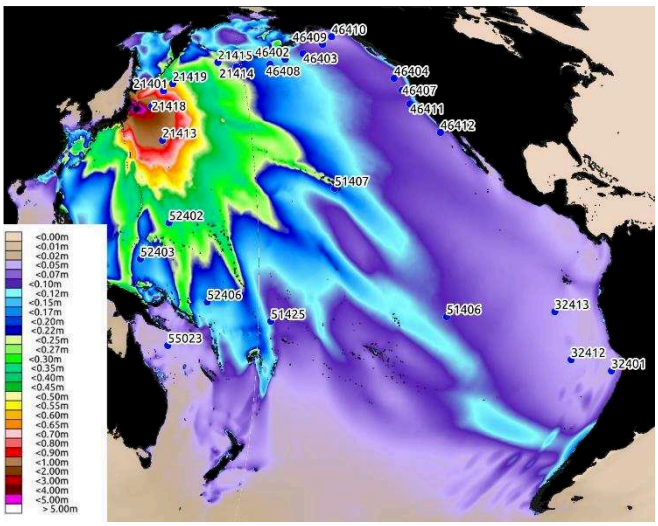

Figure 8. Maximum water level recorded in the Pacific after the event. Only active buoys are presented on the map.

The comparison between the results of the TELEMAC-2D models (using the 3 different faults configurations) are presented in the Table IV and in the Figure 9. Out of the 28 buoys that recorded a tsunami signal, 24 DART buoys were kept for the comparison in the following figures. In fact, for some buoys we couldn't filter out properly the tide constituents in the signal, due to too much noise or missing patches in the data signal.

The signal has been upsampled and "detided" using a simple low-pass filter. The upsampling was necessary because of the difference in frequency acquisition between DART's normal sampling time (15 min) and their Tsunami Response Mode sampling (15 seconds).

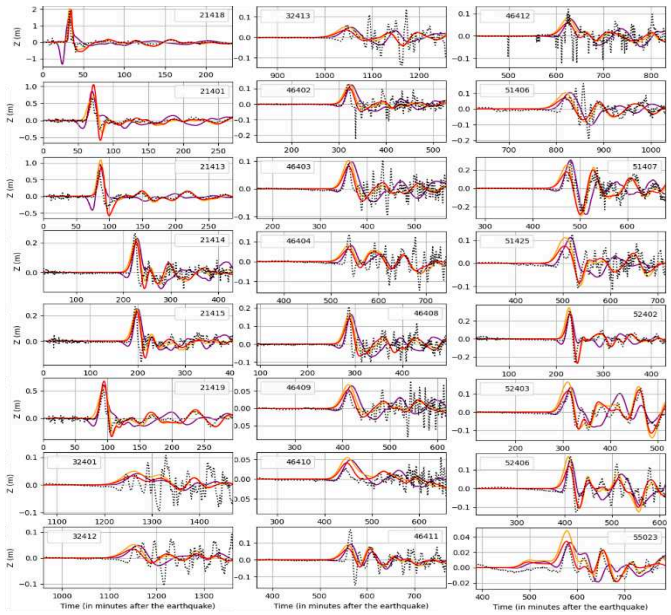

Figure 9. Comparison between the modeled free surface for all configurations (Fuji 2011 in red, Yamasaki 2018 in yellow and Romano 2012 in purple) and the measured free surface (dashed black line).

Table IV Comparison between the different model configuration and the measures at the DART buoys locations.

DART Buoy No	Distance (km)	a (m) measured	a (m) modelled using source by Fuji (2011)		a (m) modelled using source by Romano (2012)		a (m) modelled using source by Yamasaki (2018)	
21401	961	0,66	1,05	58%	**0,70**	5%	0,86	29%
21413	1190	0,77	**0,88**	15%	1,09	42%	0,96	25%
21414	3063	0,26	0,20	-23%	0,23	-14%	**0,23**	-13%
21415	2655	0,27	0,23	-15%	0,25	-8%	**0,25**	-6%
21418	507	1,87	**1,96**	5%	2,05	10%	1,42	-24%
21419	1279	0,54	0,68	27%	**0,56**	4%	0,61	13%
32401	16023	0,11	0,03	-70%	**0,05**	-54%	0,04	-62%
32412	14762	0,11	0,03	-69%	**0,05**	-53%	0,05	-56%
32413	13430	0,05	0,04	-27%	0,05	8%	**0,05**	0%
46402	4343	0,13	0,10	-21%	**0,13**	-3%	0,12	-6%
46403	4820	0,10	0,08	-21%	**0,10**	-2%	0,10	-5%
46404	6988	0,14	0,06	-54%	**0,08**	-40%	**0,08**	-40%
46407	7221	0,20	0,07	-66%	0,09	-57%	**0,09**	-55%
46408	3930	0,21	0,14	-33%	**0,17**	-21%	**0,16**	-21%
46409	5334	0,08	0,05	-32%	**0,07**	-13%	0,07	-17%
46410	5578	0,06	0,04	-31%	**0,05**	-9%	0,05	-19%
46411	7467	0,18	0,07	-63%	0,09	-51%	0,09	-49%
46412	8380	0,12	0,06	-51%	**0,08**	-33%	0,08	-37\%
51406	10768	0,16	0,07	-57%	0,10	-37%	**0,10**	-36%
51407	6142	0,30	0,20	-32%	0,25	-15%	**0,31**	4%
51425	6761	0,13	0,07	-40%	**0,11**	-11%	0,11	-10%
52402	3100	0,31	0,28	-11%	0,34	10%	**0,29**	-8%
52403	3784	0,13	0,12	-8%	0,17	25%	**0,14**	3%
52406	5320	0,17	0,12	-31%	**0,17**	-1%	0,15	-12%
55023	5961	0,03	0,03	14%	0,05	60%	**0,03**	9%

a. Comparison of the modelled and measured tsunami heights, as shown on Figure 9. In the column Distance, nuances of blue show the most distant DART buoys. For the comparisons, Green shows the best agreements and red the worst.

B. Discussion

1) Difference between the sources

The model results compare differently (Table IV) depending on the wave form used to initiate the model (Table III), and depending on the location of the buoy used for comparison.

Romano 2012 has an overestimated rundown prior to the first crest for the set of buoys nearest to the epicentre (DART 21418, DART 21401 and DART 21413) but the same rundown becomes appropriate in the Alaskan-Aleutian Islands sector (DART 46402, DART 46403 and DART 46408) or in Hawaii (DART 51407).

The Fuji 2011 configuration has the right crests in the vicinity of the tsunami but the rundown after the first wave is too important in the vicinity (DART 21401 and DART 21413, which are location between 900 km and 1100 km of the epicentre) of the tsunami and then becomes too weak in the far field.

The Yamasaki 2018 configuration has the best match overall and also is the one having the most accurate estimation for the waves/perturbations happening after the first tsunami hit.

2) Limitation of the use of TELEMAC-2D

Although the results of the three different fault models are slightly different, another immediate deduction is that there is better match between the model and the observation in the vicinity of the tsunami.

The further away from the tsunami source, the worse the model appears to match with measurements. The DART buoys offshore from the Californian coast (46404 and 46411) or from the Chilean coast (32401, 32412 and 32413) illustrate well the problem. The modelled incident waves have a longer wavelength than the ones measured (at least twice as long).

The increasing deviation we observe along the travelled distance is most likely due to the non-dispersive equations used to propagate the tsunami waves using TELEMAC-2D as we used the wave equation (default since v8p2).

Whilst this could be overcame using TELEMAC-3D the authors felt that the community would have benefitted from the present work which explores the use of TELEMAC-2D for modelling of some of the largest global tsunamis and identifies strengths and limitations of the use of this model for this purpose. The authors nevertheless intend to move onto the use of TELEMAC-3D as it represents the most obvious next step for the on-going development of the larger project of modelling the world oceans. Since the beginning, our approach has been that of increasing the level of complexity of the modelling gradually at every step of the project.

C. Other case studies

Whilst this paper presents only the results obtained modelling the most documented event, further information can be gathered from the next set of figures showing the max

tsunami-induced water elevation generated by the events enumerated in Table I.

1) Central Chile 2010

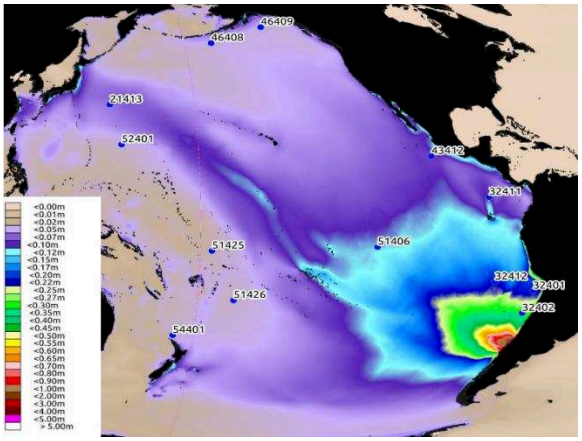

Figure 10. Maximum water level in the Pacific after the Chilean tsunami of 2010. Only the active buoys during the event are presented on the map.

2) Illapel, Chile 2015

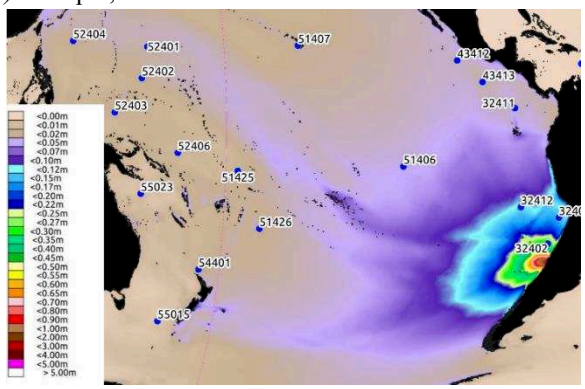

Figure 11. Maximum water level in the Pacific after the Chilean tsunami of 2015. Only the active buoys durting the event are presented on the map.

3) Samoa, 2009

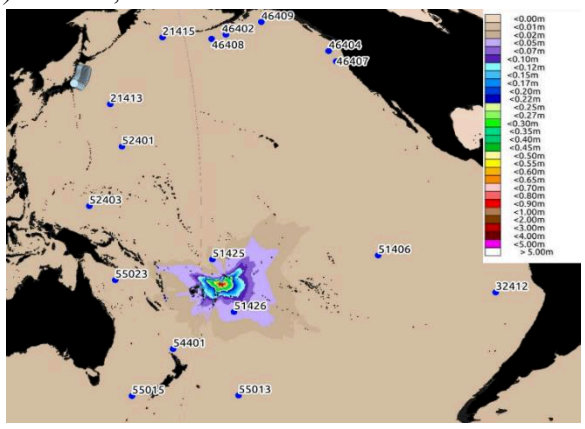

Figure 12. Maximum water level in the Pacific after the tsunami of Samoa in 2009. Only the active buoys during the event are presented on the map.

VI. RUNNING TIDES AND TSUNAMIS

The modification of the source code for the implementation of the active generation of tsunamis in TELEMAC-2D has permitted to add a temporal dimension for the triggering of the tsunami (thanks to the parameters t_i or initial activation time of the rupture fault). The following figure will just show – as a proof of concept – that multiple process can be handled in TELEMAC-2D i.e. tides and tsunamis simultaneously.

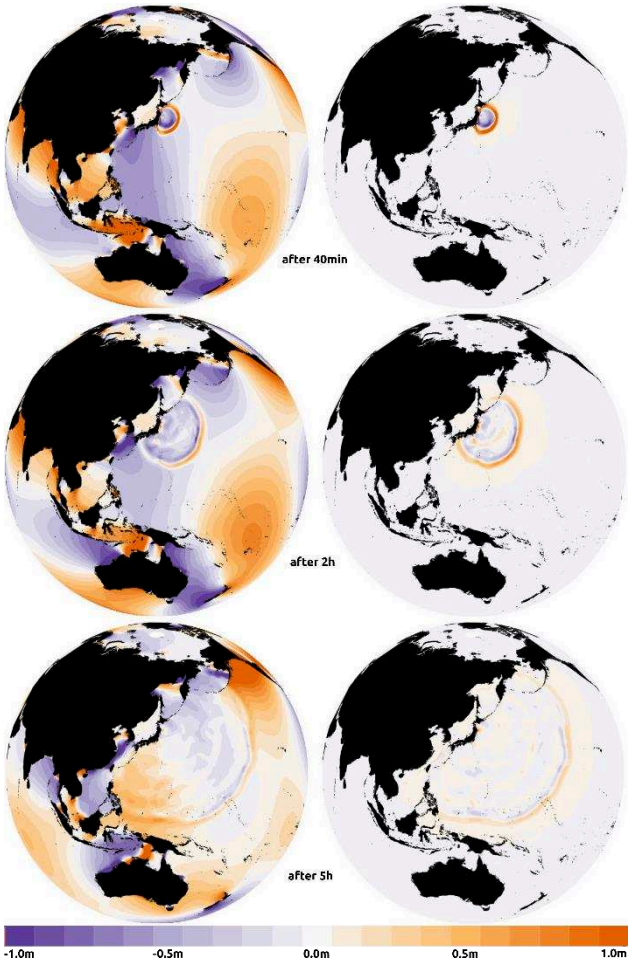

Figure 13. Snapshot comparison between the results with (insets on the left) and without (insets on the right) TIDE GENERATING FORCE. 40min (top), 2 hours (center) and 5 hours (bottom) after the earthquake

VII. PERSPECTIVES

A. TELEMAC-3D

As mentioned previously in the discussion of the results from the modelling, TELEMAC-3D is the next logical step for tsunami applications. In fact, a non-hydrostatic option is available in the code to solve equations that include the dynamic pressure allowing the resolution of the shorter wavelengths [18]. This feature will avoid having too much dispersion of tsunami waves in order to have a better estimation at the far-field locations. TELEMAC-3D will also enable a better representation of runups.

B. Runups

The three dimensionality that brings TELEMAC-3D will enhance the modelling of runups over complex coastlines. The non-hydrostatic option (mentioned in the last paragraph) will model with more accuracy tsunami surges over the shallower parts of the seabed, like trenches or steep slopes. Depending on the resolution of the bathymetric data, the estimation of surges and the modelling of inundations at the coastlines will also be possible.

The twin paper presented for this conference [19] will develop more on the on-going developments related to tsunamis runup using TELEMAC-3D.

ACKNOWLEDGEMENT

This research is being carried out as part of the SmartWave Project, funded by Regione Sicilia within the POR2014/20 EU framework. Authors wish to acknowledge the contributions of F. Oliva, A. De Prisco, S. Leo, D. D'Elia, F. Simonelli.

REFERENCES

[1] J.C. Galland, N. Goutal, J.M. Hervouet, "TELEMAC: A new numerical model for solving shallow water equations", Advances in Water Resources, 1991, Volume 14, I. 3.

[2] J.M. Hervouet, R. Ata, User manual of open software TELEMAC-2D, Report, EDF-R&D, 2017, http://www.opentelemac.org/, ISBN:9780470035580.

[3] J. Weston, A.M.G. Ferreira, G. J. Funning, Joint earthquake source inversions using seismo-geodesy and 3-D earth models, Geophysical Journal International, Volume 198, Issue 2, August, 2014, Pages 671–696, https://doi.org/10.1093/gji/ggu110

[4] T. Saillour, G. Cozzuto, F. Ligorio, G. Lupoi, S.E. Bourban, Modeling the world oceans with TELEMAC. In: A.W. Breugem, L. Frederickx, T. Koutrouveli, K. Chu, R. Kulkarni, B. Decrop, Proceedings of the papers submitted to the 2020 TELEMAC-MASCARET User Conference October 2021. Antwerp: International Marine and Dredging Consultants (IMDC), 2021, S. 86-91.

[5] National Geophysical Data Center / World Data Service: NCEI/WDS Global Historical Tsunami Database. NOAA National Centers for Environmental Information. doi:10.7289/V5PN93H7 [01/09/2022]

[6] Flanders Marine Institute (VLIZ); Intergovernmental Oceanographic Commission (IOC): Sea level station monitoring facility, 2022. Accessed at https://www.ioc-sealevelmonitoring.org on 2022-09-01 at VLIZ. DOI: 10.14284/482

[7] S.E. Bourban, M.S. Turnbull, A.J. Cooper, The Earth by TELEMAC. In: C. Dorfmann, G. Zenz, Proceedings of the XXIVth TELEMAC-MASCARET User Conference, 17 to 20 October 2017, Graz University of Technology, Austria. Graz: Graz University of Technology. 2017, S. 1-8.

[8] Y. Okada, Internal deformation due to shear and tensile fault in a half space. Bulletin of the Seismological Society of America. 92, 1992, 1018-1040.

[9] Y. Yamazaki, K. F. Cheung, Z. Kowalik, T. Lay, G. Pawlak, NEOWAVE. In Proceedings and Results of the NTHMP Model Benchmarking Workshop, 2012, pp. 239–302. Galveston, TX: NOAA Special Report.

[10] G. Davies, F. Romano, S. Lorito, Global dissipation models for simulating tsunamis at far-field coasts up to 60 hours post-earthquake, multi-site tests in Australia, Front. Earth Sci ., 2020, 8 , 497.

[11] NTHMP. Technical Report. Proceedings and results of the 2011 NTHMP model benchmarking workshop. National Tsunami Hazard Mitigation Program, NOAA Special Report, 2012.

[12] D. Dutykh, D. Mitsotakis, X. Gardeil and F. Dias, On the use of finite fault solution for tsunami generation problems. Theoretical and Computational Fluid Dynamics, Springer Verlag, 2013, 27 (1), pp.177-199. 10.1007/s00162-011-0252-8. hal-00509384v3

[13] Y. Fujii and K. Satake, Slip Distribution and Seismic Moment of the 2010 and 1960 Chilean Earthquakes Inferred from Tsunami Waveforms and Coastal Geodetic Data, 2013, Pure Appl. Geophys. 170, 1493–1509.

[14] P.K. Ravi, Computer Simulation of 2011 East Japan. Earthquake and Tsunami. UTRIP-2013. 10th June - 19th July, 2013. https://www.s.u-tokyo.ac.jp/en/utrip/archive/2013/pdf/07RaviPrabhatKumar.pdf

[15] F. Romano et al. Clues from joint inversion of tsunami and geodetic data of the 2011 Tohoku-oki earthquake, 2012, Sci Rep 2, 385.

[16] Y. Yamazaki, K.F. Cheung and T. Lay, A Self-Consistent Fault Slip Model for the 2011 Tohoku Earthquake and Tsunami. J. Geophys. Res. Solid Earth 123, 1435–1458, 2018.

[17] D. Mitsotakis, Boussinesq systems in two space dimensions over a variable bottom for the generation and propagation of Tsunami waves. Mathematics and Computers in Simulation, 2009, 80(4):860–73.7

[18] A. Cooper, G. Cuomo, S.E. Bourban, Testing TELEMAC-2D suitability for tsunami propagation from source to near shore. In: S.E. Bourban, N. Durand, J.M. Hervouet, Proceedings of the XIXth TELEMAC-MASCARET User Conference 2012, 18 to 19 October 2012, St Hugh's College, Oxford. Oxfordshire: HR Wallingford. S. 89-92

[19] G. Cozzuto, T. Saillour and G. Lupoi, Tsunamis induced run-up benchmarking with Telemac3D, unpublished.